Journal of Open Humanities Data

Tracing Changes in Shape of Historical Artefacts Across Time Using 3D Scans: A New Computational Approach

RESEARCH PAPER

GIOVANNI MARIA PALA
LISANDRA S. COSTINER
*Author affiliations can be found in the back matter of this article

ubiquity press

ABSTRACT

This paper pioneers a new computational approach for the study of changes in shape of objects across time. Previously, such a study was undertaken by scholars using a purely visual approach and relied on images of objects or in-person observations. This paper's approach is based on 3D scans of historical artefacts. Sample points are extracted from these 3D scans and the distance between analogous points across different objects is computed using an approximation of the Wasserstein metric, namely the Sinkhorn distance. In this paper, the approach is demonstrated on a small set of ancient Greek vessels of the Krater, Pelike, and Kylix types, as the variation in their shapes across time is well known to archaeologists. Results offer, for the first time, a way of quantifying differences between objects. Benefits of this approach lie in its ability to quantify change, to study complex 3D material, and to analyse large datasets of objects, opening the possibility of constructing new large-scale studies of object shape across time and geographical regions. These have a range of applications in art history, archaeology, digital humanities, museology and extended reality studies.

CORRESPONDING AUTHOR:
Giovanni Maria Pala
Magdalen College, University of Oxford, Oxford, GB
giovanni.pala@magd.ox.ac.uk.

KEYWORDS:
shape comparison; 3D models; digital humanities; archaeology; digital art history; Sinkhorn distance.

TO CITE THIS ARTICLE:
Pala, G. M., & Costiner, L. S. (2022). Tracing Changes in Shape of Historical Artefacts Across Time Using 3D Scans: A New Computational Approach. *Journal of Open Humanities Data*, 8: 14, pp. 1–13. DOI: *https://doi.org/10.5334/johd.61*

DOI: 10.5334/johd.61

(1) INTRODUCTION

The study of forms and styles as embodying the cultural concerns of a particular historical moment has been at the centre of several disciplines, most importantly archaeology and art history. In archaeology, morphology, or the study of shapes, has been used to group, analyse, and date artefacts (Algrain & Tonglet, 2021; Conkey & Hastorf, 1990). One of the best-known adherents to this approach was John Beazley (1885–1970) who used the shapes of ancient Greek, or Attic, pots and their painting styles to categorise, date, and attribute vessels to particular painters (Beazley, 1925). In art history, one of the first proponents of the categorisation of art based on style was Johann Joachim Winckelmann (1717–1768), whose interest in archaeology led him to chart progressions within Greek and Roman art (Winckelmann, 1764/2006). Concern with forms, or formalism, features prominently in the theories of early art historian Alois Riegl (1858–1905), who argued that forms embodied the spirit of a particular age (Riegl, 1901/1985), and Heinrich Wölfflin (1864–1945), who saw the development of form as cyclical (Wölfflin, 1915/2015). More recently, the theory found voice in Henri Focillon's (1881–1943) *La vie des formes* (1934), and its further development by George Kubler (1912–1996) in *The shape of time*, who proposed new ways of historical sequencing based on continuous change across time (Kubler, 1962). This study inscribes itself within this intellectual tradition. It proposes a new way of quantifying changes in shape and of exploring connections between objects using, for the first time, a computational technique.

In the field of computer science, more specifically computer vision, shape registration, or the computation of correspondences across shapes, remains a challenge (Díez et al., 2015). This technique compares shapes to assess their degree of similarity to pre-existing archetypes. These comparisons rely on the concept of 'relatedness' or 'distance' between shapes: how similar (close) or how dissimilar (distant) they appear to be. The method can be applied to the problem of defining the relative similarity of historical objects. Our approach uses an approximation of the Wasserstein metric (Villani, 2009: 105–123) to quantify changes in shape. The Wasserstein metric, also known as the Earth Mover's Distance (EMD), in its simplest terms, is the 'cost' of moving a collection of points from one shape into another.

Although the approach outlined here can be employed on any group of historical artefacts, in this paper we use a curated dataset of ancient Greek pottery as a case study. Ancient Greek pottery has been chosen as it follows a clear trajectory in the evolution of shapes—pots created in different time periods and locations tending to exhibit different features. Many studies in the field of archaeology have focused particularly on these changes (for an overview of literature, see Algrain & Tonglet, 2021). Variations in the shapes of these objects have been quantified by scholars visually, using differences in form to delineate distinct moments in the chronology of pottery production (Richter & Milne, 1935; Kerschner & Schlotzhauer, 2005). Visual analysis is so fundamental to the study of ancient Greek pottery that large archives, such as the Beazley Archive at the University of Oxford, have been created to document surviving objects and assist in their study (Beazley Archive).

Moving away from the traditional technique of using drawings to document vessel profiles (Bloesch, 1940; Kathariou, 2017), archaeologists have recently begun exploring computational techniques. These include profile-based shape matching (Smith et al., 2014; Martínez-Carrillo, 2008), the use of digital signatures (Koutsoudis & Chamzas, 2009), pose normalisation and segmentation (Koutsoudis et al., 2010), and reducing 3D models to depth-map images using compact 2D shape descriptors (Koutsoudis & Chamzas, 2011)—all valuable techniques for classifying unknown 3D models of Greek pots.

The current approach relies on 3D scans of historical objects, complex digital material which has seen only limited use in scholarship, and proposes a novel methodology for quantifying changes in form. This will enable the study of trends and progressions, as well as highlight aberrations, or divergences. It is important to note that this paper makes no claim as to the trajectory of changes in form and acknowledges that some historical objects may not follow consistent patterns and may resist strict typological categorisation. The value of the approach lies in its ability to quantify, for the first time, form changes, eliminating the subjectivity of the observer, to study complex 3D material, such as object scans, and to analyse large datasets.

DOI: 10.5334/johd.61

(2) DATASET

As no central repository of 3D models of historical artefacts currently exists, the present study relies on a dataset which was curated by the authors from 3D models found on the Sketchfab platform (*https://sketchfab.com*). This was supplemented by additional scans, conducted in the course of this study, of original ancient Greek pottery held in the Ashmolean Museum in Oxford. The Sketchfab models downloaded were chosen based on two criteria. Firstly, models were identified which could be downloaded freely for study purposes. Secondly, the model had to be a scan of an actual museum object and be linked, whenever possible, to the original museum catalogue record. This ensured that the object was not a fabrication, namely a 3D model created by an individual onto which the texture of a historical object was mapped. Museum catalogue data linked to each object also allowed us to record key information related to the vessel's origin, dating and measurements. Three vessel types were chosen, the Bell Krater, a large pot used for the dilution of wine with water, the Kylix, a wine drinking cup, and the Pelike, a container probably used for wine (***Figure 1***). This choice was driven by the availability of models of these vessel types. Every effort was made to identify models of objects produced in the same location, Greece, although the Pelike examples were unearthed in other ancient Greek settlements. We also aimed to include objects produced in different time periods to test potential changes in designs. These restrictions significantly limited the number of models which could be employed in this study resulting in a small dataset.

Figure 1 (from left to right) Image of a Krater (in this paper, K4), Kylix (Y3), and Pelike (P1), which have been analysed as part of this study. The objects are held by the Ashmolean Museum in Oxford under inventory numbers AN1944.15, AN1947.109, and AN1960.1200, respectively. Images © Ashmolean Museum, University of Oxford.

This small dataset was supplemented by a number of 3D scans of original ancient Greek pots held in the collection of the Ashmolean Museum in Oxford. The models were created using photogrammetry and the photographs were processed into a 3D model using the Agisoft Metashape software.[1] Although the size of the corpus used in this study is limited, it is sufficient for testing the approach proposed and shows the value of this study as a proof of concept. The approach can also be scaled over a large dataset.

As can be seen visually from point clouds of the 3D models used in this study (***Figures 2–4***), the objects chosen to represent each vessel type exhibit variations in shape. ***Figure 2*** depicts the four Kraters included in the dataset, arranged in chronological order. The oldest object (K1) dates to the fifth century BC, K2 to the mid-fifth century BC, K3 to the first half of the fourth century BC, and K4 to the second quarter of that century (ca. 375-350 BC). Information about each digital model, the size of each object and its catalogue description are included in ***Appendix 1***.

Figure 3 depicts the four Kylikes which form part of the dataset, arranged in chronological order. Most of the Kylikes studied are of one shape, known either as type A or type II (Richter & Milne, 1935: figs. 159–162). Given the small size of 3D models of this type available, we had to supplement this dataset with one cup of another type, type I (Richter & Milne, 1935: figs. 152–154). Labelled as Y1, it dates from the sixth century BC. Other cups in the dataset were produced in ca. 530 BC (Y2), in ca. 530-500 BC (Y3), and ca. 500 BC (Y4).

1 We are currently in conversation with the Ashmolean Museum to upload the dataset on the Oxford Cabinet platform (*www.cabinet.ox.ac.uk*), to facilitate further studies.

DOI: 10.5334/johd.61

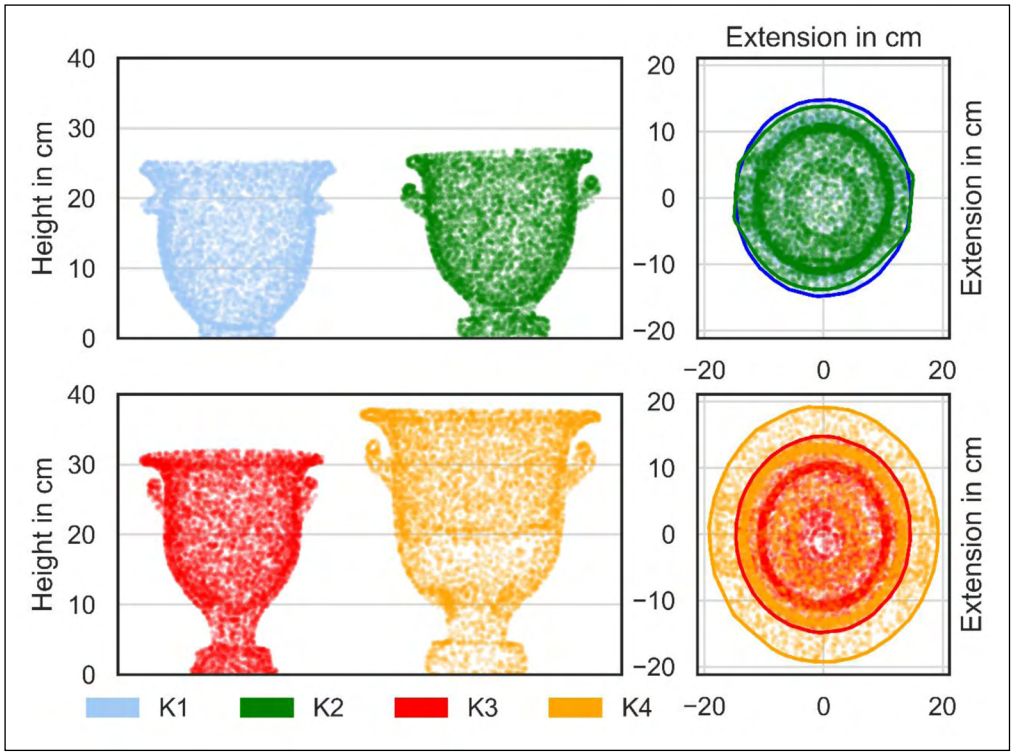

Figure 2 Lateral and top views of the Kraters studied, as represented by point clouds. The vessels have been arranged chronologically and labelled K1 (oldest object) to K4 (youngest). The extension in cm graphs represent the top views of the Kraters nestled within one another. The thicker lines enclose the outer edges of each vessel.

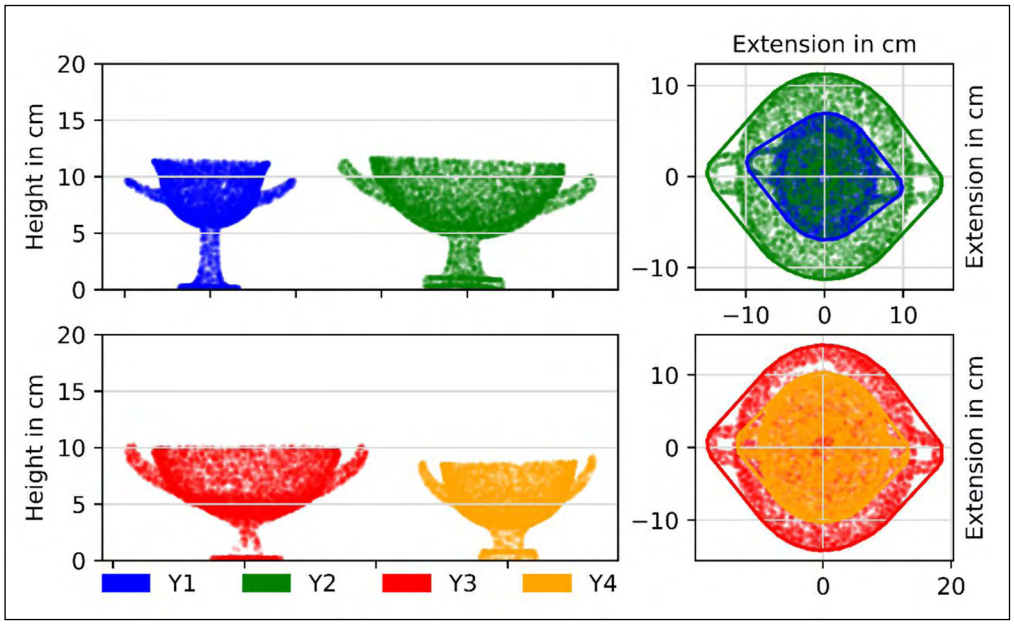

Figure 3 Lateral and top views of the Kylikes studied, as represented by point clouds. The vessels have been arranged chronologically and labelled Y1 (oldest object) to Y4 (youngest). The extension in cm graphs represent the top views of the Kylikes nestled within one another. The thicker lines enclose the outer edges of each vessel.

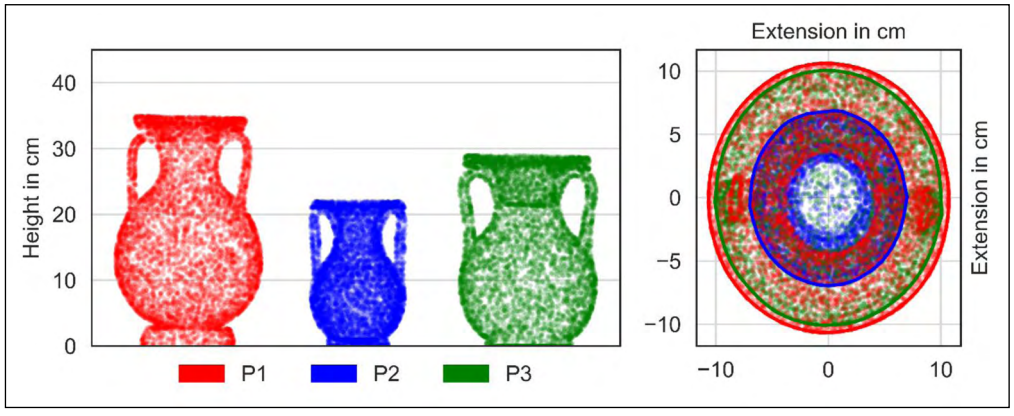

Figure 4 Lateral and top views of the Pelikai studied, as represented by point clouds. The vessels have been arranged chronologically and labelled P1 (oldest object) to P3 (youngest). The extension in cm graphs represent the top views of the Pelikai nestled within one another. The thicker lines enclose the outer edges of each vessel.

Due to the difficulty of sourcing models, the Pelikai dataset consists of only three models. They were objects excavated from Greek colonies. P1 is a Pelike dating from fourth century BC Apulia. P2 was likewise created in the fourth century BC, but was unearthed in the Greek Black Sea colony of Kerch, while P3 derives from the same region but is thought to have been created ca. 300 BC.

(3) METHOD

To analyse the dataset, the following procedure was used. From each 3D model of a historical object in the dataset, the mesh was loaded. From the mesh, a random sample of vertices of a given size was extracted. The sample of vertices constitutes a cloud of points distributed around the vessel mesh (*Figure 6*). This is the most basic representation of the object and is useful in comparing different vessel forms. The chosen sample size for this study was 1,000 points, which allows for computational manageability while also adequately approximating each vessel shape. As the sample size of points grows, there are increasingly small gains in terms of precision but the complexity of the calculations increases more than linearly $O(n^2)$ in the computation of the Sinkhorn distance (or larger in the case of the Wasserstein distance). This is clearly illustrated in *Figure 5*, where the gains of increased sample sizes for a Sinkhorn distance converge to a relatively stable Sinkhorn value at roughly 1,000 to 2,000 sampled points for the models used in this study. The unstable values for low sample sizes are due to the approximation characteristic of the Sinkhorn distance and the different sampling configurations of each run: as each new sample is a resample of larger distributions, every set of points will be slightly different.

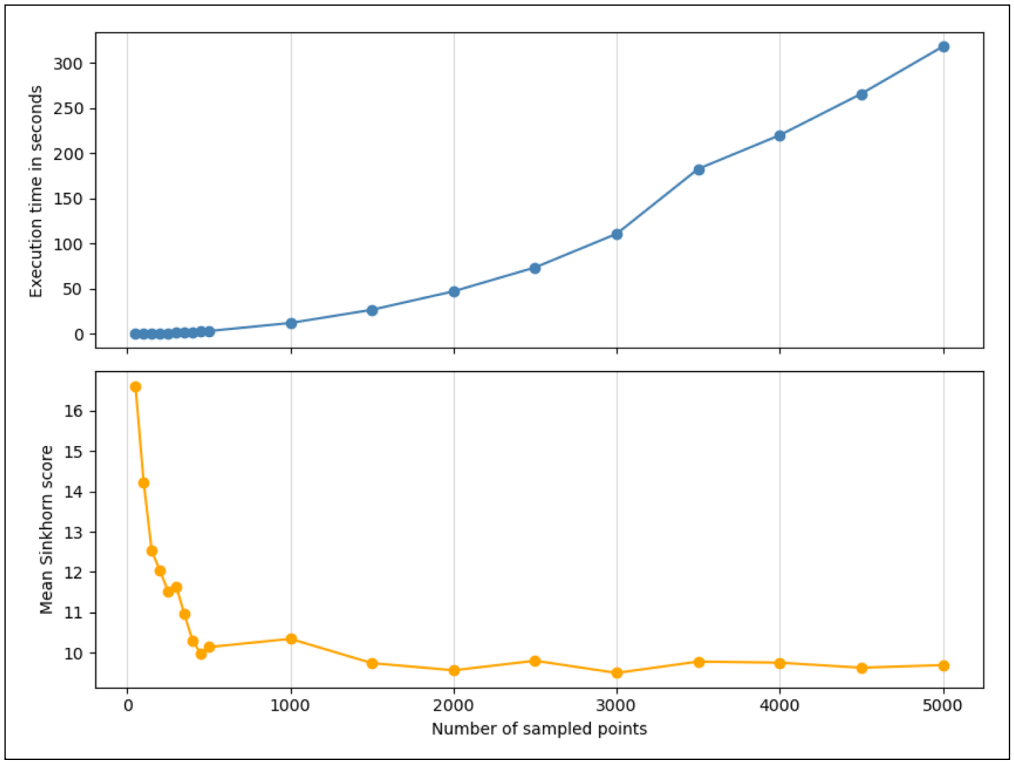

Figure 5 The mean Sinkhorn distance and computational time between models Y1 and Y2 as the number of points sampled from each model increases. The figure illustrates how, as the number of points sampled from a 3D model increases, the efficiency gains decrease. As the number of points sampled increases, the computational time (in blue) increases exponentially; at the same time, the mean value of the Sinkhorn score (in orange), after a quick convergence, remains stable.

All models were pre-processed to reflect their real-world proportions and a consistent orientation. The vessels were roto-translated and centred so that the handles and orientations were standardised across models. They were also scaled to reflect their proportions, derived from the height of the original objects. Once the pre-processing was completed, the models were compared through metrics that measured the distance between the distribution of points from one object and those from a second object.

This study relies on an approximation of the Wasserstein metric, following an approach developed by Marco Cuturi (Cuturi, 2013). The approximated distance is called a Sinkhorn distance, after the Sinkhorn-Knopp algorithm used in a passage of the new approach. The

current study uses this technique, which relies on a smoothing parameter, in our case set at e^{-3}. A pre-existing suite was deployed to implement the algorithm.[2]

The use of the Wasserstein metric, and its computationally more approachable twin, the Sinkhorn distance, has been proposed recently and tested as a solution to the problem of defining a distance between 3D shapes (Shi & Wang, 2020; Su et al., 2015). One of the main benefits of using a Wasserstein metric rests on the existence of a solution to the pairwise comparison between shapes, and its capacity to capture discrepancies in the objects' features. Its main drawback is the high computational cost, which, in the standard Wasserstein metric, has computational complexity $\mathrm{O}(n^3 \log n)$, reduced in the case of the Sinkhorn distance to a still challenging $\mathrm{O}(n^2)$ (Genevay et al., 2019). The letter n is the number of supports of the probability distribution used in the Wasserstein distance, in our case points in 3D space. Computational onerousness is a challenge of many optimal transport solutions applied to shape comparison, but the Wasserstein metric, as we will show, is useful, especially if we frame our problem as one of closely related masses. Because the Wasserstein distance is not the only possible approach or metric that can be applied to computing differences between masses, other distances will also be explored in this paper as a means of comparison, namely the Chamfer and the Hausdorff distances.

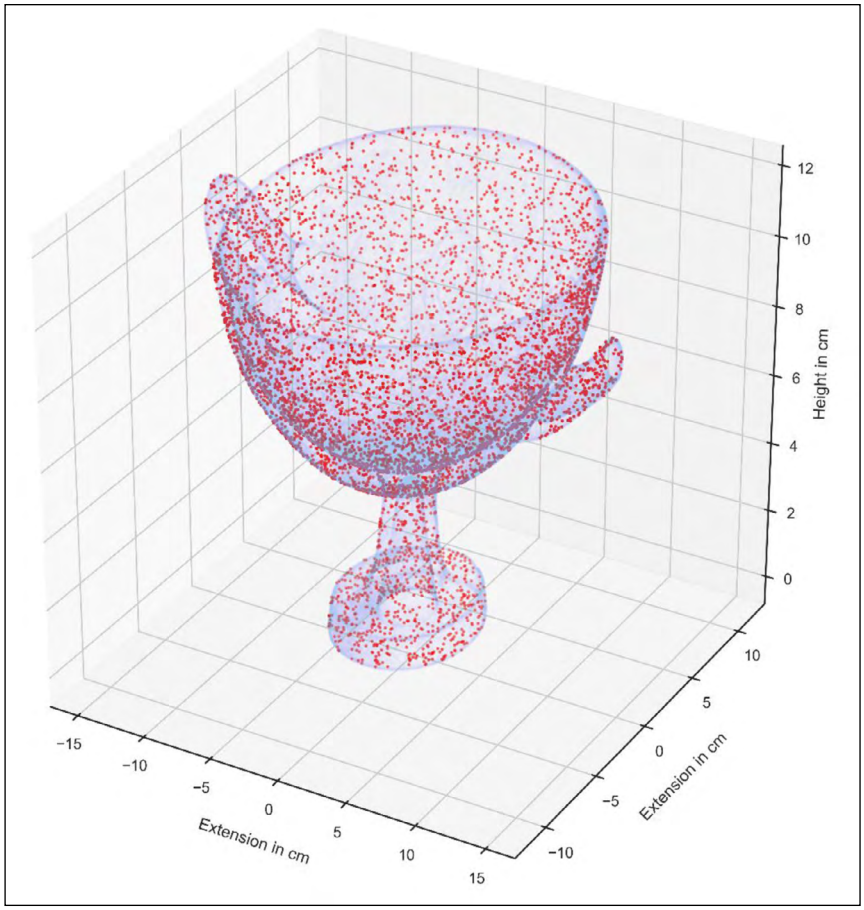

Figure 6 Kylix model, displaying the total mesh vertices (blue) and sampled vertices (red). The figure displays the vertices of the mesh of a Kylix model (Y1) used in the dataset (light blue, high transparency) and the random subsample of one thousand points (red, larger).

In its most simple formulation, the Wasserstein metric is a distance function between two equal masses (measures) distributed on a metric space (our 3D space). These distributions can be read as a probability distribution (i.e., total mass is one) over all the points (the support of the distribution). The distance between the two distributions is computed as the result of an optimisation problem which seeks to minimise the cost of moving the mass of one distribution into the shape of the other.

In discrete terms, we have two distributions of points A and B with $x_i \in A$ and $y_j \in B$ denoting the i^{th} and j^{th} point of either distribution. We assume that each point is the realisation of a sampling exercise with equal probability (our random sampling) such that the individual probability

2 'Point Cloud Utils (pcu) - A Python library for common tasks on 3D point clouds', URL: *https://github.com/fwilliams/point-cloud-utils*.

DOI: 10.5334/johd.61

mass is a fraction of the total number of points. That is, for a point p_j in A, its probability is $p_j = 1/|A|$ where $|A|$ is the number of elements of A. This means that the masses are equally split (and the points equally probable). The cost of moving the mass from a point x_i to a point y_i is given by a distance $d(x_i, y_j)$ on the metric space (e.g., the Euclidean distance) (***Figure 7***). The original formulation (Monge's problem) defined the Wasserstein metric between A and B as the minimum total cost to move all the masses $x_i \in A$ to the points $y_j \in B$. The approach we use here follows the Kantorovich-Kolmogorov formulation which allows for split masses. This approach can be shown to be a solution to the Monge's problem and is symmetric: two desirable qualities. With split masses, for any mass of size $m_{xy} \in \mathbb{R}$ strictly moving from x to y (hence the condition $m_{xy} \geq 0$)), we define the Wasserstein Metric $W(A, B)$ between the two distributions as the solution to

$$\min \sum_{x,y \in A \times B} d(x,y) \cdot m_{xy}$$

over all possible m_{xy} with $x \in A$, $y \in B$; subject to the conditions of complete redistributions of the masses, for each fixed $x \in A$, $\sum_{y \in B} m_{xy} = p_x$, and for each fixed $y \in B$, and $\sum_{x \in A} m_{xy} = p_y$, with $\sum p_A = \sum p_B$. This latter condition allows for the splitting of the masses, which are completely removed from the points in A, and their redistribution such that, at the end of the process, the sums of the allocated m_{xy} at every point y in B add up to the expected $p_y = 1/|B|$. To allow for comparability, the Wasserstein metric can be normalised by division with the least common multiple between $(|A|, |B|)$. This, however, is unnecessary in our case of equally-sized clouds of points.[3]

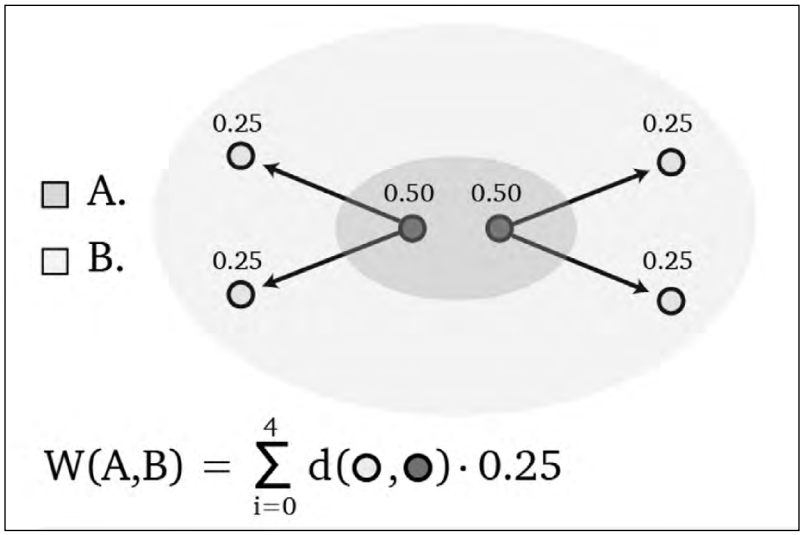

Figure 7 A representation of the Wasserstein metric on a Euclidean space. The Wasserstein metric, W, joins two discrete distributions A and B by equally splitting masses (adding up to 1 in each case) on A and B and solving an optimal transport plan to redistribute them from A into B.

The Wasserstein metric is beneficial in the current comparative approach as it can synthetise into one 'number' the dissimilarity between two distributions (shapes): the greater the difference between two shapes (or dissimilarity), the greater the cost (value) to reposition their points. Despite its benefits, the Wasserstein metric has a number of disadvantages or limitations. A prominent one, in our case, is that the optimal solution of the plan that solves the problem can re-shuffle points at great distances. This renders it difficult to point to specific features of an object (e.g., differences in the shape of the handles or of the neck of a vessel) that are leading to the higher total redistribution cost. In short, the algorithm does not facilitate the pinpointing of features that are most dissimilar between one vessel (or shape) and another. However, as a general measure of similarity, and conversely dissimilarity, the metric is useful.

Computing the Sinkhorn distances is another step in the pipeline. They provide some additional information about the direction and intensity of the optimal redistribution plan between the objects (see ***Figure 8***). The comparison produced is a series of pairwise distances that can be used to assess the relative closeness or similarity between shapes.

3 We are indebted to Jeremy Kun, 'Earth Mover's Distance'. *Math ıProgramming*, https://jeremykun.com/tag/wasserstein-metric/ for the simple formulation of a mathematically complex metric. This informed the formulation used in this paper.

DOI: 10.5334/johd.61

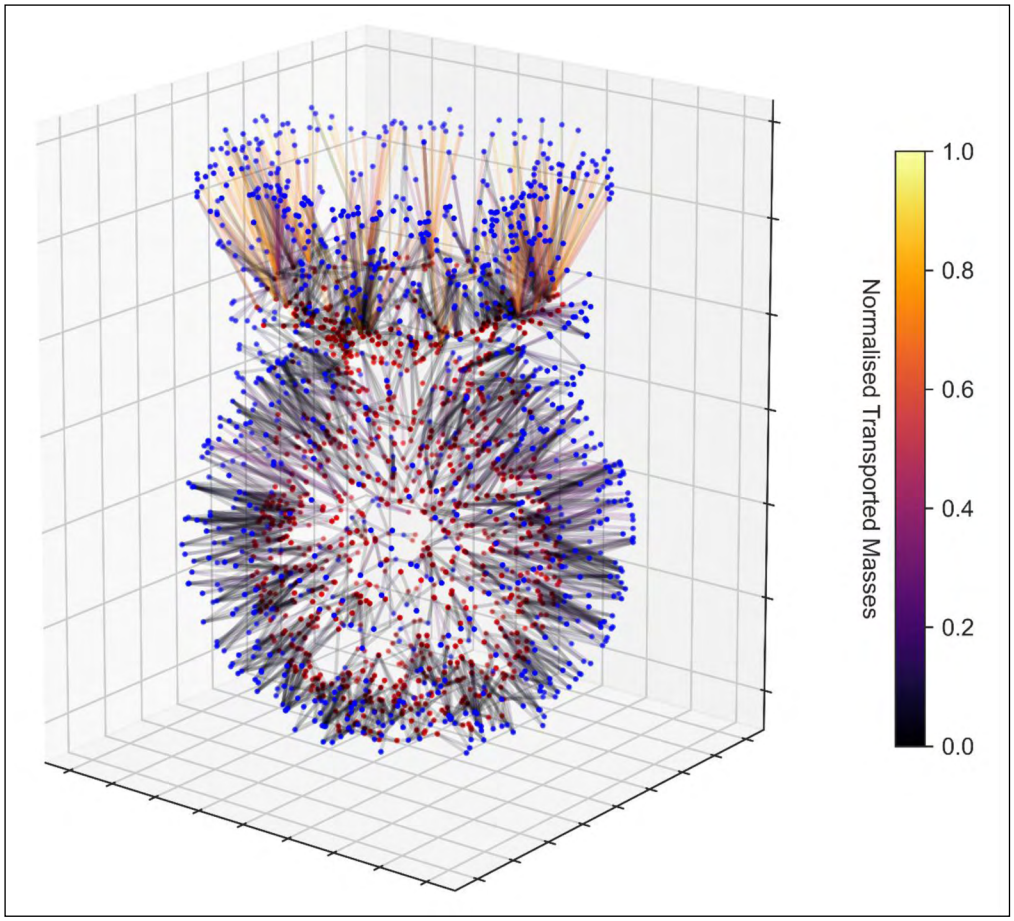

Figure 8 Transport plans, coloured by their normalised total cost, between two cloud points of Pelikai P1 and P2. One cloud of points is in blue directed towards the other, smaller, in red. The image clearly shows that the most extreme and different elements are those that need to be moved at a greater distance and thus have a larger cost (yellow-orange colour).

(4) RESULTS

Table 1 lists the Sinkhorn distances between the different objects in the Krater, Kylix, and Pelike sets. The Sinkhorn distance calculations appear to match a visual analysis of the vessels. For example, in the Krater set, Krater K1 and K2 have the smallest Sinkhorn distance (normalised to 0.16) and are thus the most similar objects in this dataset. When the shapes of the objects are compared (*Figure 2*), one can easily see that the two objects resemble each other closely in both shape and dimensions. K4, a Krater of much larger size, is the most dissimilar (the normalised Sinkhorn distance between K2 and K4 being 1). Similar comparisons can be seen for the other vessel types.

These results accord with the chronology of the vessels and their development. K1 and K2 date from the fifth century BC while K4 was created a century later, around the second quarter

Table 1 Sinkhorn distances computed between each pair of objects of a particular type (Krater, Kylix and Pelike). The original values for vessels K1 to K4, Y1 to Y4, and P1 to P3 are the total pixel distances weighted by their split mass as defined by the optimal transport problem. For comparability, a normalised version is produced which displays the distances from 0 to 1, obtained by dividing each distance by the largest recorded distance within each vessel type.

KRATER					KYLIX					PELIKE			
SINKHORN ORIGINAL VALUES													
	K1	**K2**	**K3**	**K4**		**Y1**	**Y2**	**Y3**	**Y4**		**P1**	**P2**	**P3**
K1		2470	5878	13892	**Y1**		10149	28013	10089	**P1**		10297	19146
K2	2470		3213	15413	**Y2**	10149		4285	892	**P2**	10297		3189
K3	5878	3213		10687	**Y3**	28013	4285		3200	**P3**	19146	3189	
K4	13892	15413	10687		**Y4**	10089	892	3200					
NORMALISED SINKHORN													
	K1	**K2**	**K3**	**K4**		**Y1**	**Y2**	**Y3**	**Y4**		**P1**	**P2**	**P3**
K1		0.16	0.38	0.90	**Y1**		0.36	1.00	0.36	**P1**		0.54	1.00
K2	0.16		0.21	1.00	**Y2**	0.36		0.15	0.03	**P2**	0.54		0.17
K3	0.38	0.21		0.69	**Y3**	1.00	0.15		0.11	**P3**	1.00	0.17	
K4	0.90	1.00	0.69		**Y4**	0.36	0.03	0.11					

of the fourth century (ca. 375–350 BC). Analysing objects as a cloud of points also allows the vessels to be superimposed so that differences between objects can be visualised in the round, facilitating the interpretation of results (***Figure 9***). Because of the limited nature of the dataset, this analysis serves to show the viability of the approach. A larger dataset would be needed to draw conclusions about the trajectory of shape design over time in these vessel types. In a larger dataset, we would expect to be able to see and analyse changes which have been recorded in literature, such as the transformation of the Kylix cup over time to become wider and shallower, with a progressively shorter and more slender foot (Richter & Milne, 1935: figs. 159–162).

To be able to compare and determine the suitability of the Sinkhorn distance in this study, we also analysed our dataset using two other distances, the Chamfer distance and the Hausdorff distance (***Table 2***). The Chamfer distance is the average distance between each point on one vessel and its nearest equivalent from a second vessel, while the Hausdorff distance is the greatest of the distances between a point on one object and the closest point in the other object. As can be seen in ***Table 2***, the results accord, broadly, with those of the Sinkhorn approach. The extremes, the most similar and most dissimilar object pairs remain unaltered. It must be noted, however, that, because other distances are not designed to satisfy the same requirements as the Wasserstein metric, the morphological elements they emphasise may be different and require more in-depth study and a careful interpretation.

Some of the patterns that emerge with the Wasserstein distance can also be seen in the results of the other distances, especially in the extreme values. The Hausdorff distance may be more sensitive to local differences. This can be seen when comparing the differently shaped handles of the Kylikes, shown in ***Figure 10***.

Table 2 Krater, Kylix, and Pelike alternative distances. The Chamfer distance is the average distance between each vessel's point and the nearest point from a second vessel and vice-versa. The Hausdorff distance is the greatest of the distances obtained from a point in one vessel to the closest point in a second vessel and vice-versa. The partial Hausdorff or Chamfer distances, not mentioned here, are the intermediate step: they do not consider the other direction and are therefore non-symmetric. For comparability, a normalised version is produced which displays the distances from 0 to 1, obtained by dividing each distance by the largest recorded distance per vessel type.

KRATER					KYLIX					PELIKE			
CHAMFER ORIGINAL VALUES													
	K1	**K2**	**K3**	**K4**		**Y1**	**Y2**	**Y3**	**Y4**		**P1**	**P2**	**P3**
K1		5.21	7.81	8.66	**Y1**		9.27	15.00	10.78	**P1**		10.87	14.41
K2	5.21		5.50	10.22	**Y2**	9.27		6.61	3.18	**P2**	10.87		5.44
K3	7.81	5.50		10.12	**Y3**	15.00	6.61		6.13	**P3**	14.41	5.44	
K4	8.66	10.22	10.12		**Y4**	10.78	3.18	6.13					
NORMALISED CHAMFER													
	K1	**K2**	**K3**	**K4**		**Y1**	**Y2**	**Y3**	**Y4**		**P1**	**P2**	**P3**
K1		0.51	0.76	0.85	**Y1**		0.62	1.00	0.72	**P1**		0.75	1.00
K2	0.51		0.54	1.00	**Y2**	0.62		0.44	0.21	**P2**	0.75		0.38
K3	0.76	0.54		0.99	**Y3**	1.00	0.44		0.41	**P3**	1.00	0.38	
K4	0.85	1.00	0.99		**Y4**	0.72	0.21	0.41					
HAUSDORFF ORIGINAL VALUES													
	K1	**K2**	**K3**	**K4**		**Y1**	**Y2**	**Y3**	**Y4**		**P1**	**P2**	**P3**
K1		3.21	4.54	8.60	**Y1**		5.62	8.84	4.23	**P1**		4.82	7.09
K2	3.21		4.15	8.82	**Y2**	5.62		4.17	2.64	**P2**	4.82		3.79
K3	4.54	4.15		6.44	**Y3**	8.84	4.17		5.49	**P3**	7.09	3.79	
K4	8.60	8.82	6.44		**Y4**	4.23	2.64	5.49					
NORMALISED HAUSDORFF													
	K1	**K2**	**K3**	**K4**		**Y1**	**Y2**	**Y3**	**Y4**		**P1**	**P2**	**P3**
K1		0.36	0.51	0.98	**Y1**		0.64	1.00	0.48	**P1**		0.68	1.00
K2	0.36		0.47	1.00	**Y2**	0.64		0.47	0.30	**P2**	0.68		0.53
K3	0.51	0.47		0.73	**Y3**	1.00	0.47		0.62	**P3**	1.00	0.53	
K4	0.98	1.00	0.73		**Y4**	0.48	0.30	0.62					

DOI: 10.5334/johd.61

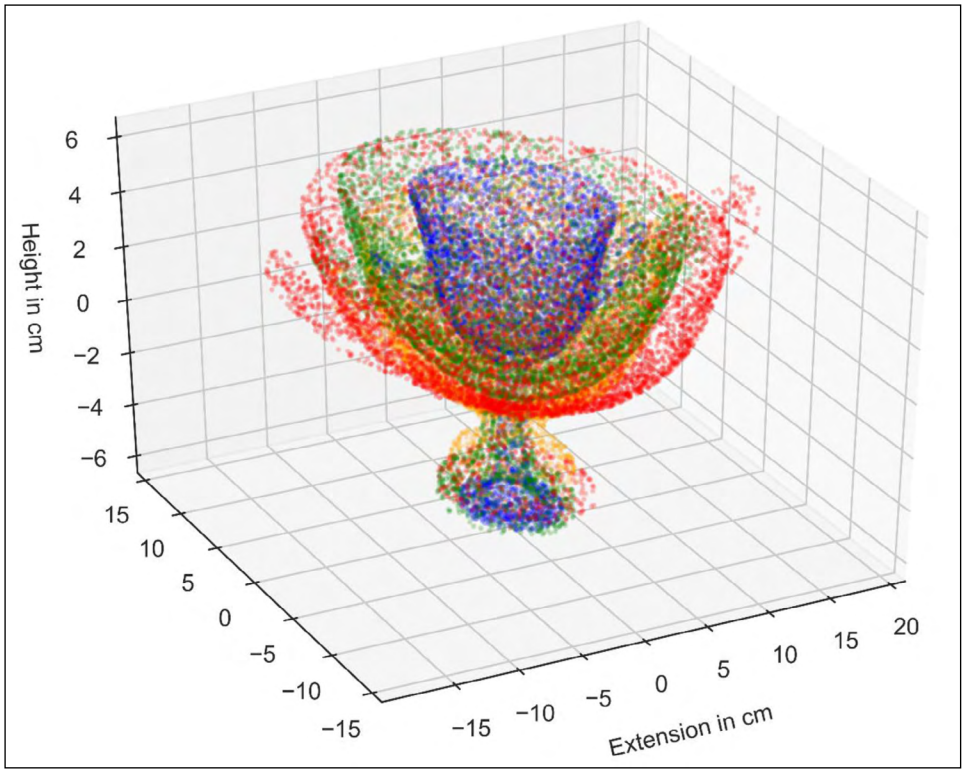

Figure 9 Kylix point clouds superimposed at scale. The image displays Y1 (blue), Y2 (green), Y3 (red), and Y4 (orange), scaled to preserve the proportions of the originals and nested within each other. The scale is in cm, and the origin is in the centre of the vessels.

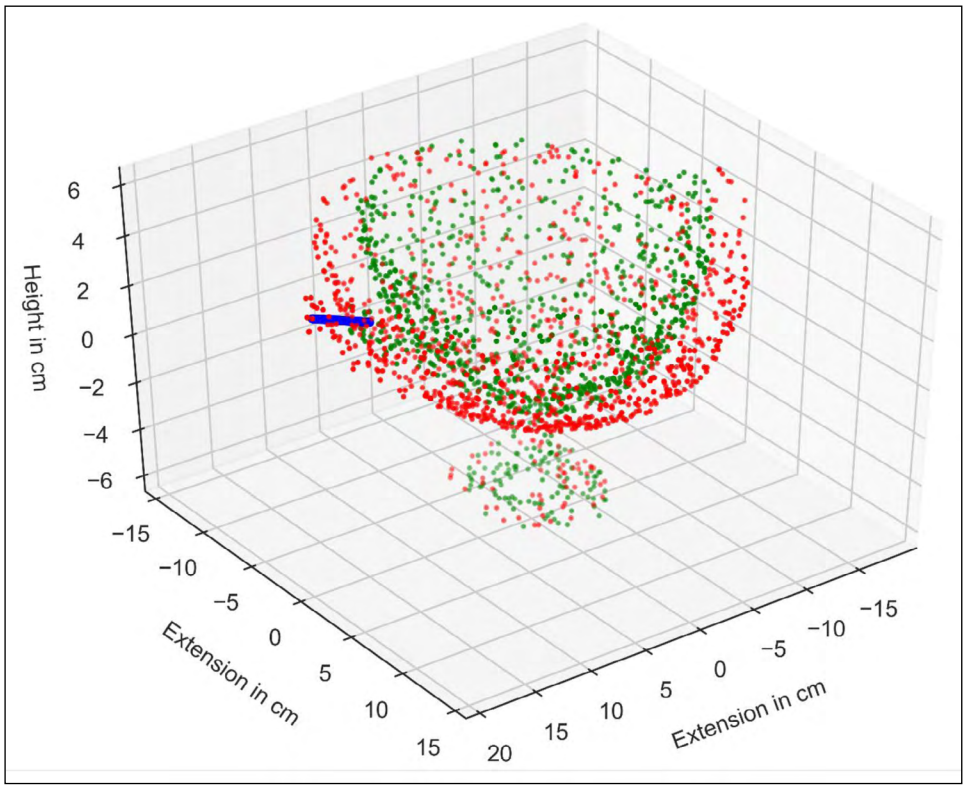

Figure 10 Points where the partial Hausdorff distance between Y2 and Y3 lays. The image displays the sub-samples of Y2 in green and Y3 in red. The Hausdorff distance is represented in blue (left handle of the objects). As can be seen in this example, the feature that tends to define the Hausdorff distance in Greek vessels is the handle. The models are centred so that the origin of the 3D space is in the centroid of the cloud of points.

(5) CONCLUSION

This study has outlined a new computational approach for quantifying changes in the shape of historical objects over time. Although the dataset is too small to draw any conclusions about the historical or art historical trajectory of the objects analysed here, it does serve to illustrate the value of the computational approach in comparing objects. When paired with information about an object's size, it allows for precise analysis, supplanting the typical visual and subjective means of recording changes. In time, 3D models can also be produced that capture the inside of each vessel. This would record the thickness of each vessel's walls, which may also prove important in later comparisons.

The method can be scaled to large datasets of 3D objects scans where changes can be computed automatically, without the need for human intervention. The benefits of this approach lie in its ability to quantify changes in form, to study complex 3D material, to analyse large datasets, and to record variations in shape which are imperceptible to the human eye. As museums and cultural institutions move to digitise their collections in three dimensions, this approach opens new possibilities for the large-scale study of form. In particular, affinities can help establish connections between objects, highlight patterns of influence or stylistic exchange, or periods of stylistic continuity and rupture (renascence and disjunction) in the history of form, areas of interest to art historians and archaeologists. Results can also be visualised in mixed reality formats, used in immersive pedagogy, museology and outreach.

In the particular case of Greek vessels, the current approach, if undertaken on a large dataset can help illuminate more specific research questions. Some Attic potters prided themselves in the ability to produce exact reproductions of vessels, and this approach would immediately highlight such instances enabling the grouping of pots, and their assignment to individual potters (Langner, 2013). Other studies have shown how it is not similarities but certain inconsistencies that are the mark of other artisans, markers which again can be easily distinguished through the current approach (Euwe, 1996: 70–71). More broadly, the large study of shapes, it has been argued, can help illuminate greater questions, such as the organisation of workshops in ancient Greece, networks of collaboration, and intercultural interactions in the ancient Mediterranean (Algrain & Tonglet, 2021). The method can also be used in the dating of the vast corpus of sparsely decorated vases, lacking painting – a feature that has been widely used in assigning provenance and in dating.

Future avenues in which we plan to expand this study include the enlargement of the dataset with a greater number of models of a particular vessel type produced across a large chronological period. The dataset could also be expanded to include other types of Greek vessels, created in different parts of the Mediterranean. Over time, the approach can be applied to any type of object, and especially to those which are not symmetrical. As the method is scalable, this would enable the mapping of changes in shape across time and geographical locations, allowing scholars to build a new history of form and design.

APPENDIX 1: DATASET

OBJECT ID	SOURCE OF 3D MODEL	OBJECT RECORD (MUSEUM CATALOGUE)	HEIGHT:
KRATER			
Krater: K1	*https://sketchfab.com/3d-models/bell-krater-6fc57b2d891047b396b31f961f0a0259*	Stockholm, Medelhavsmuseet, NM Ant 0008. *https://collections.smvk.se/carlotta-mhm/web/object/3100844*	25.3 cm.
Krater: K2	*https://sketchfab.com/3d-models/19223galt112-cratera-8f84a276a97742cdb912e3deb1d4f512*	Madrid, Museo Arqueológico Nacional, 1922/3/GAL/T11/2. *http://ceres.mcu.es/pages/Main?idt=107590&inventary=1979%2F70%2FGAL%2FT11%2F2&table=FMUS&museum=MAN#.WiazrDczeqI.email*	27 cm
Krater: K3	*https://sketchfab.com/3d-models/bell-krater-2ab07881be8f41fa8adee94236ec869a*	Stockholm, Medelhavsmuseet, NM Ant 0014. *https://collections.smvk.se/carlotta-mhm/web/object/3100845*	32 cm
Krater: K4	3D scan.	Oxford, Ashmolean Museum, AN1944.15. *https://collections.ashmolean.org/collection/browse-9148/object/88737*	38 cm.
KYLIX			
Kylix: Y1	*https://sketchfab.com/3d-models/kylix-greek-ffe14358f8ce44b6bc201341e7dc8bfe*	Private collection.	11.5 cm
Kylix: Y2	*https://sketchfab.com/3d-models/kylix-drinking-cup-eye-cup-495e835bbb214120958dbcd730f48fb5*	Cambridge, MA, Harvard Art Museum, 1925.30.19. *https://www.harvardartmuseums.org/collections/object/292633*	11.7 cm
Kylix: Y3	3D scan	Oxford, Ashmolean Museum, AN1947.109 *https://collections.ashmolean.org/object/471063*	10.4 cm

(Contd.)

OBJECT ID	SOURCE OF 3D MODEL	OBJECT RECORD (MUSEUM CATALOGUE)	HEIGHT:
Kylix: Y4	3D scan	Oxford, Ashmolean Museum, AN1960.1219 *https://collections.ashmolean.org/object/470924*	9.4 cm
PELIKE			
Pelike: P1	3D scan	Oxford, Ashmolean Museum, AN1960.1200 *https://collections.ashmolean.org/collection/browse-9148/object/153886*	35.2 cm
Pelike: P2	*https://sketchfab.com/3d-models/red-figure-pelike-d2e78236a1b54f41bf2e115a779a966f*	Kraków, Archaeological Museum, MAK/3591 *https://muzea.malopolska.pl/en/objects-list/629*	22 cm
Pelike: P3	*https://sketchfab.com/3d-models/pelike-f440061d2c604c2b88139063033b9d8a*	Kraków, Archaeological Museum, MNK XI-A-361 *https://muzea.malopolska.pl/en/objects-list/2466*	29 cm

ACKNOWLEDGEMENTS

We would like to thank Dr Andrew Shapland, Curator of Bronze Age and Classical Greece at the Ashmolean Museum in Oxford, and his team for facilitating the scanning of ancient Greek vessels in their collection. We thank Richard Smith, of the University of Oxford, for undertaking the photogrammetry and model processing. We are also grateful to Dr Anestis Koutsoudis, of the Athena Research and Innovation Centre (Xanthi's Division), for consulting with us on this research. This study was supported by the Oxford X-Reality Hub.

COMPETING INTERESTS

The authors have no competing interests to declare.

AUTHOR AFFILIATIONS

Giovanni Maria Pala *orcid.org/0000-0002-7100-5429*
Magdalen College, University of Oxford, Oxford, GB

Lisandra S. Costiner *orcid.org/0000-0002-2841-8957*
Harvard University Center for Renaissance Studies, Villa I Tatti, Florence, IT

REFERENCES

Algrain, I., & **Tonglet, D.** (2021). Studying the shapes of Greek vases: historiography and new methodologies. *Archeologia e Calcolatori*, *32*(2), 65–82.

Beazley Archive, Classical Art Research Centre, University of Oxford. URL: *https://www.beazley.ox.ac.uk*.

Beazley, J. D. (1925). *Attische Vasenmaler Des rotfigurigen Stils*. Tübingen: J.C.B. Mohr.

Bloesch, H. (1940). *Formen attischer Schalen von Exekias bis zum Ende des Strengen Stils*. Bern: Benteli.

Conkey, M., & **Hastorf, A.** (1990). *The uses of style in archaeology*. Cambridge: Cambridge University Press.

Cuturi, M. (2013). Sinkhorn distances: Lightspeed computation of optimal transport. *Advances in Neural Information Processing Systems*, *26*, 2292–2300.

Díez, Y., Roure, F., Lladó, X., & **Salvi, J.** (2015). A qualitative review on 3D coarse registration methods. *ACM Computing Surveys* 47(3), 1–36. DOI: *https://doi.org/10.1145/2692160*

Euwe, J. (1996). The potters of the Nolan amphorae in Sicily: Criteria for attributions. In G. Rizza (Ed.), *I vasi attici ed altre ceramiche coeve in Sicilia. Atti del convegno internazionale (Catania, Camarina, Gela, Vittoria 1990)* (Vol. II, pp. 67–80). Catania: Centro di studio sull'archeologia greca.

Focillon, H. (1934). *Vie des formes*. Paris: Ernest Leroux.

Genevay, A., Chizat, L., Bach, F., Cuturi, M., & **Peyré, G.** (2019). Sample complexity of Sinkhorn divergences. *Proceedings of the 22nd International Conference on Artificial Intelligence and Statistics (AISTATS), Naha, Okinawa, Japan*, *PMLR 89*, 1574–1583.

Kathariou, K. (2017). Moving Bloesch's methodology one century forward: Challenges and perspectives. In L. Cappuccini, C. Leypold, & M. Mohr (Eds.), *Fragmenta Mediterranea. Contatti, tradizioni e innovazioni in Grecia, Magna Grecia, Etruria e Roma. Studi in onore di Christoph Reusser* (pp. 217–230). Sesto Fiorentino: All'Insegna del Giglio.

Kerschner, M., & **Schlotzhauer, U.** (2005). A new classification system for east Greek pottery. *Ancient West & East*, 4(1), 1–56. DOI: *https://doi.org/10.1163/9789047416692_003*

Koutsoudis, A., & **Chamzas, C.** (2009). 3D pottery shape similarity matching based on digital signatures. *Proceedings of the Computer Applications to Archaeology*, 166–171.

Koutsoudis, A., & **Chamzas, C.** (2011). 3D pottery shape matching using depth map images. *Journal of Cultural Heritage*, *12*, 128–133. DOI: *https://doi.org/10.1016/j.culher.2010.12.003*

Koutsoudis, A., Pavlidis, G., Liami, V., Tsiafakis, D., & **Chamzas, C.** (2010). 3D Pottery content-based retrieval based on pose normalisation and segmentation. *Journal of Cultural Heritage*, *11*(3), 329–338. DOI: *https://doi.org/10.1016/j.culher.2010.02.002*

Kubler, G. (1962). *The shape of time: Remarks on the history of things*. New Haven: Yale University Press.

Kun, J. (2018). 'Earth Mover's Distance'. *Math ⁄ Programming*. URL: *https://jeremykun.com/tag/wasserstein-metric/.*

Langner, M. (2013). Grundlagen der Chronologie spätrotfiguriger Vasen aus Athen. *Bulletin Antieke Beschaving*, *88*, 127–170.

Martínez-Carrillo, A. (2008). Computer applications in archaeological pottery: A review and new perspectives. *Proceedings of the 36th CAA Conference, Budapest, 2–6 April 2008*, 394–401.

Point Cloud Utils (pcu). URL: *https://github.com/fwilliams/point-cloud-utils.*

Richter, G., & **Milne, M.** (1935). *Shapes and names of Athenian vessels.* New York: Metropolitan Museum of Art.

Riegl, A. (1985). *Late Roman art industry* (R. Winckes, Trans.). Rome: Giorgio Bretschneider. (Original book published 1901).

Shi, J., & **Wang, Y.** (2020). Hyperbolic Wasserstein distance for shape indexing. *IEEE Transactions on Pattern Analysis and Machine Intelligence*, *42*(6), 1362–1376. DOI: *https://doi.org/10.1109/TPAMI.2019.2898400*

Sketchfab. URL: *https://sketchfab.com*.

Smith, N. G., Karasik, A., Narayanan, T., Olson, E., Smilansky, U., & **Levy, T. E.** (2014). The pottery informatics query database: A new method for mathematic and quantitative analyses of large regional ceramic datasets. *Journal of Archaeological Method and Theory*, *21*, 212–250. DOI: *https://doi.org/10.1007/s10816-012-9148-1*

Su, Z., Wang, Y., Shi, R., Zeng, W., Sun, J., Luo, F., & **Gu, X.** (2015). Optimal mass transport for shape matching and comparison. *IEEE Transactions on Pattern Analysis and Machine Intelligence*, *37*(11), 2246–2259. DOI: *https://doi.org/10.1109/TPAMI.2015.2408346*

Villani, C. (2009). *Optimal transport: Old and new*. Berlin: Springer. DOI: *https://doi.org/10.1007/978-3-540-71050-9*

Winckelmann, J. (2006). *The history of the art of antiquity* (H. F. Mallgrave, Trans.). Los Angeles: Getty Research Institute. (Original work published 1764).

Wölfflin, H. (2015). *Principles of art history: The problem of the development of style in early modern art*. (J. Blower, Trans.). Los Angeles, CA: Getty Research Institute. (Original book published 1915).

TO CITE THIS ARTICLE:
Pala, G. M., & Costiner, L. S. (2022). Tracing Changes in Shape of Historical Artefacts Across Time Using 3D Scans: A New Computational Approach. *Journal of Open Humanities Data*, 8: 14, pp. 1–13. DOI: *https://doi.org/10.5334/johd.61*

Published: 20 May 2022